

**Optimizing Model Complexity for System Level Models of Fuel  
Cell Power Systems**

Karthik Subramanyan, and Urmila M. Diwekar\*

Vishwamitra Research Institute -

Center for Uncertain Systems, Tools for Optimization and Management

34, N.Cass Ave.  
Westmont, IL 60607  
urmila@vri-custom.org

ID#: 17565  
Password#: 822876

Prepared for AIChE Annual Meeting 2005  
Cincinnati, OH

\* Corresponding Author

## **Abstract**

Optimization problems can be computationally intensive and therefore, they often use simple reduced order models for system level designs. However, this simplicity can induce uncertainties in the performance indices. In a multi-objective context, the trade-off between different objectives can change significantly due to these uncertainties. This paper presents a case study of a fuel cell based hybrid power system design where different levels of fuel cell models are used. Uncertainties are characterized and quantified in these models using experimental data. Effect of these uncertainties on multi-objective trade-off surfaces is analyzed. It has been shown that improving model complexity results in uncertainty reduction and helps in obtaining better representation of trade-off surfaces. An optimal level of fuel cell model complexity has been identified and improving the model beyond this would not provide any significant enhancement of predicted results for the hybrid power plant design under focus.

## Nomenclature

SOFC: Solid Oxide Fuel Cell

PEMFC: Proton Exchange Membrane Fuel Cell

MOP: Multi-objective Optimization

ASU: Air Separation Unit

HRSG: Heat Recovery Steam Generator

$U_f$  : Fuel Utilization in the fuel cell

$H_2^{reacted}$  : the total moles of hydrogen reacted in the fuel cell ( $\text{kgmol hr}^{-1}$ )

$CH_4^{in}$  : the moles of methane entering the fuel cell ( $\text{kgmol hr}^{-1}$ )

$CO^{in}$  : the moles of carbon monoxide entering the fuel cell ( $\text{kgmol hr}^{-1}$ )

$H_2^{in}$  : the moles of hydrogen entering the fuel cell ( $\text{kgmol hr}^{-1}$ )

$O_2^{in}$  : the moles of oxygen entering the fuel cell ( $\text{kgmol hr}^{-1}$ )

$O_2^{out}$  : the moles of oxygen exiting the fuel cell ( $\text{kgmol hr}^{-1}$ )

ISOFC: the current in the SOFC (A)

$cdsofc$  : the SOFC current density ( $\text{mA cm}^{-2}$ )

$cdim$ : the ratio of the mean current density to the minimum current density of SOFC

$eref$ : the reference Nernst potential (V)

$ecell$ : the operating cell voltage (V)

$hd$ : the heat duty of the RGIBBS reactor representing the SOFC (Btu/hr)

$eloc$ : the local nernst potential (V)

$X_r$ : the reference fuel conversion

$r$ : the cell ohmic resistance ( $0.73 \text{ ohm cm}^{-2}$ ) taken from the fuel cell hand book

$cdsofc$ : the SOFC current density ( $\text{A m}^{-2}$ )

$E(cdsofc)$  : the SOFC cell voltage as a fn. of current density (V)

$E_0$  : the reference cell voltage without any losses (V);

$R_e$  : Electrolyte area-specific ohmic resistance ( $\Omega \text{ m}^{-2}$ )

$\bar{R}$  : Universal gas constant ( $=8.314 \text{ Jmol}^{-1} \text{ K}^{-1}$ )

T : Temperature (K)

F : Faraday constant ( $=96485 \text{ C mol}^{-1}$ )

K : equilibrium constant

$p_{H_2O}^I$  : Partial pressure of  $H_2O$  in the inlet stream (Pa)

$p_{H_2}^I$  : Partial pressure of  $H_2$  in the inlet stream (Pa)

$p_{O_2}^I$  : Partial pressure of  $O_2$  in the inlet stream (Pa)

$p_0$  : Atmospheric pressure (Pa)

$cdsofc_{0a}$  : anode exchange current density in SOFC ( $\text{A m}^{-2}$ )

$cdsofc_{0c}$  : cathode exchange current density in SOFC ( $\text{A m}^{-2}$ )

$l_a$  : anode thickness (m)

$D_{a(eff)}$  : effective diffusion coefficient (anode) ( $m^2 s^{-1}$ )  
 $l_c$  : cathode thickness (m)  
 $D_{c(eff)}$  : effective diffusion coefficient (cathode) ( $m^2 s^{-1}$ )  
 $p_c$  : cathode pressure (Pa)  
 $cdpem$ : current density ( $A cm^{-2}$ ).  
 $E(cdpem)$ : Cell voltage as a function of current density (V)  
 $E_0$ : reference voltage (V)  
 $cdimp$ : is the ratio of mean current density to the minimum current density of PEMFC  
OCV: open circuit voltage  
 $cdpem_0$  : exchange current density in PEMFC ( $Acm^{-2}$ )  
 $R_{cell}$  : cell resistance ( $\Omega cm^2$ )  
 $cdpem_{lim}$  : limiting current density in PEMFC ( $Acm^{-2}$ )  
 $c_{H^+}$  : fixed charge concentration ( $molcm^{-3}$ )  
 $l_m$  : wet membrane thickness (cm)  
 $cdpem_{0,Pt}$  : exchange current density per Pt surface in PEMFC ( $Acm^{-2}Pt$ )  
 $S_{Pt}$  : Catalyst surface area ( $cm^2/mg$ )  
 $W_{Pt}$  : catalyst loading ( $mg cm^{-2}$ )  
 $U_{Pt}$  : catalyst utilization  
 $D_{O_2N_2}$  : oxygen/nitrogen binary diffusion coefficient at standard conditions ( $cm^2s^{-1}$ )  
 $V_m$  : standard molar volume ( $22414 cm^3 mol^{-1}$ )  
 $l_{d+}$  : cathode gas-diffusion layer thickness (cm)  
 $x_{O_2}$  : gas-phase mole fraction of  $O_2$   
***FUT: Fuel utilization***  
***ERAT: Equivalence ratio***  
***PPEM: Pressure of the PEM (psi)***  
***FUEL: Fuel Flow ( $kgmol hr^{-1}$ )***  
***AIR: Air Flow ( $kgmol hr^{-1}$ )***  
**CAP: Capital Cost (\$/kW)**  
**COE: Cost of Electricity (c/kWh)**  
**ACEFF: Overall Efficiency**  
**CO2EM: CO<sub>2</sub> Emissions (kg/kWh)**  
**MINSOOP: Minimize Number of Single Objective Optimization Problems**  
**HSS: Hammersley Sequence Sampling**  
**LHHS: Latin Hypercube Hammersley Sampling**

**Greek Letters:**

$\eta_{Ohm}$  : Ohmic Polarization (V)

$\eta_{Act,a}$  : Anodic activation polarization (V)

$\eta_{Act,c}$  : Cathodic activation polarization (V)

$\eta_{Conc,a}$  : Anodic concentration polarization (V)

$\eta_{Conc,c}$  : Cathodic concentration polarization (V)

$\delta_{O_2}$  : ratio of Knudsen diffusion coefficients

$\eta_{dif}$  : diffusion overpotential

$\eta_{conv}$  : overpotential associated with proton transport for convection

$\omega$  : empirical constant for diffusion overpotential ( $\Omega\text{cm}^2\text{K}^{-1}$ )

$\nu$  : water velocity in membrane pores ( $\text{cm}\text{s}^{-1}$ )

$\kappa$  : membrane ionic conductivity ( $\Omega^{-1}\text{cm}^{-1}$ )

$\tau_R$  : membrane resistance/cell resistance ratio

$\varepsilon_g^d$  : gas porosity in gas-diffusion layer

$n_e$  : electrons transferred per reaction

$\eta_{act}$  = activation polarization (V)

$\eta_{conc}$  = concentration polarization (V)

## **1. Introduction**

Chemical process industries manage some of the most sophisticated and expensive engineered systems in the world, spending large amounts of money in plant design, operation, and maintenance. To achieve performance targets and at the same time reduce the number of costly pilot-scale and demonstration facilities, the designers of these process plants increasingly rely on high-fidelity computer process simulations to design and evaluate *virtual plants*. Existing commercial simulation software products used in the chemical process industries employ two main levels of model abstraction: 1) models of the overall process (a forest-level description) and 2) more detailed models of individual equipment items in the process (a tree-level description) [1]. The system level models used in the forest-level description of a chemical process tend to use simpler and reduced order models to represent modules for various reasons including: 1) speedup of computation 2) emphasis is on the overall flowsheet output rather than detailed output of individual modules. In this case, there is a trade-off between the degree of accuracy, and the speed and complexity of computation which gives rise to uncertainties in the design. One of our earlier papers concerned uncertainty analysis and multi-objective optimization [2] for the Solid Oxide Fuel Cell (SOFC)-Proton Exchange Membrane Fuel Cell (PEMFC) hybrid power plant conceptual design [3]. The plant was designed using simplified models for both the fuel cell systems. Further, the hybrid fuel cell technologies are new and futuristic. Hence the system level models used to simulate the SOFC's and PEMFC's performance had significant uncertainties in them. These individual models were found to deviate from experimental results by as much as 30%. . Also the performance curves for the fuel cell section of the flowsheet would differ depending on the materials for the anode, cathode and electrolyte. Substantiating this fact, it was found that there was a considerable difference between the deterministic and the stochastic optimization results which justified the necessity for uncertainty analysis. The focus of this paper is an extension of that work, where we reduce the uncertainties induced by the simpler fuel cell models, by employing higher level models for the PEMFC and SOFC. These models too are obviously not free from errors, but they introduce a significant improvement over the previous ones. We then perform deterministic and stochastic multi-objective optimization with the new models and compare the Pareto surfaces to the stochastic Pareto surface computed with the old models .Through this exercise, we can identify how much model complexity is sufficient in order to provide the decision maker with proper design trade-offs and optimal designs. Comparison of the degree of similarity between the trade-off surfaces would give us an idea of whether the newer models for the PEMFC and SOFC were accurate enough for the level of detail required for the plant.

The section following this introduction provides a brief overview of the SOFC-PEMFC hybrid power plant conceptual design. Section 3 explains the old and new SOFC and PEMFC models in detail and compares the corresponding

models. Section 4 discusses the uncertainty analysis of the new PEMFC and SOFC models and the stochastic multi-objective optimization (MOP) framework which is used to compute the Pareto surface. Section 5 presents the results of the optimization; analyzes and compares the trade-off surfaces computed. The final section puts forth conclusion drawn from this work. It should also be noted that the deterministic and stochastic multi-objective optimization of the flowsheet using the old fuel cell models shall henceforth be referred to as “stochastic old” and “deterministic old” respectively and analogously for the designs with new models, they shall be referred to as “deterministic new” and “stochastic new”.

## **2. Solid Oxide Fuel Cell (SOFC) – Proton Exchange Membrane Fuel Cell (PEMFC) hybrid power plant conceptual design**

This section explains the structure of each individual section of the plant in focus, which is the SOFC-PEMFC hybrid power system. Figure 1 shows the Aspen Plus flowsheet for this power plant. Only the major blocks have been depicted in the flowsheet for the purpose of clarity and the abbreviation of each section is described for each block.

**2.1 Air Separation Unit:** The purpose of this module is to separate Oxygen ( $O_2$ ) and Nitrogen ( $N_2$ ) in ambient air because the SOFC requires a pure oxygen stream. 200 lbmol/hr of ambient air ( $O_2$  21%,  $N_2$  79%) stream (AMBAIR) enters the air separation unit (ASU) represented using an Aspen Plus “two-outlet component separator” model which can split components based on specified mass flowrate of outlet streams. The two outlet streams are: OXYGEN - 28 lbmol/hr containing oxygen to the SOFC, NITROGEN - the rest 142 lbmol/hr containing 99 %  $N_2$ .

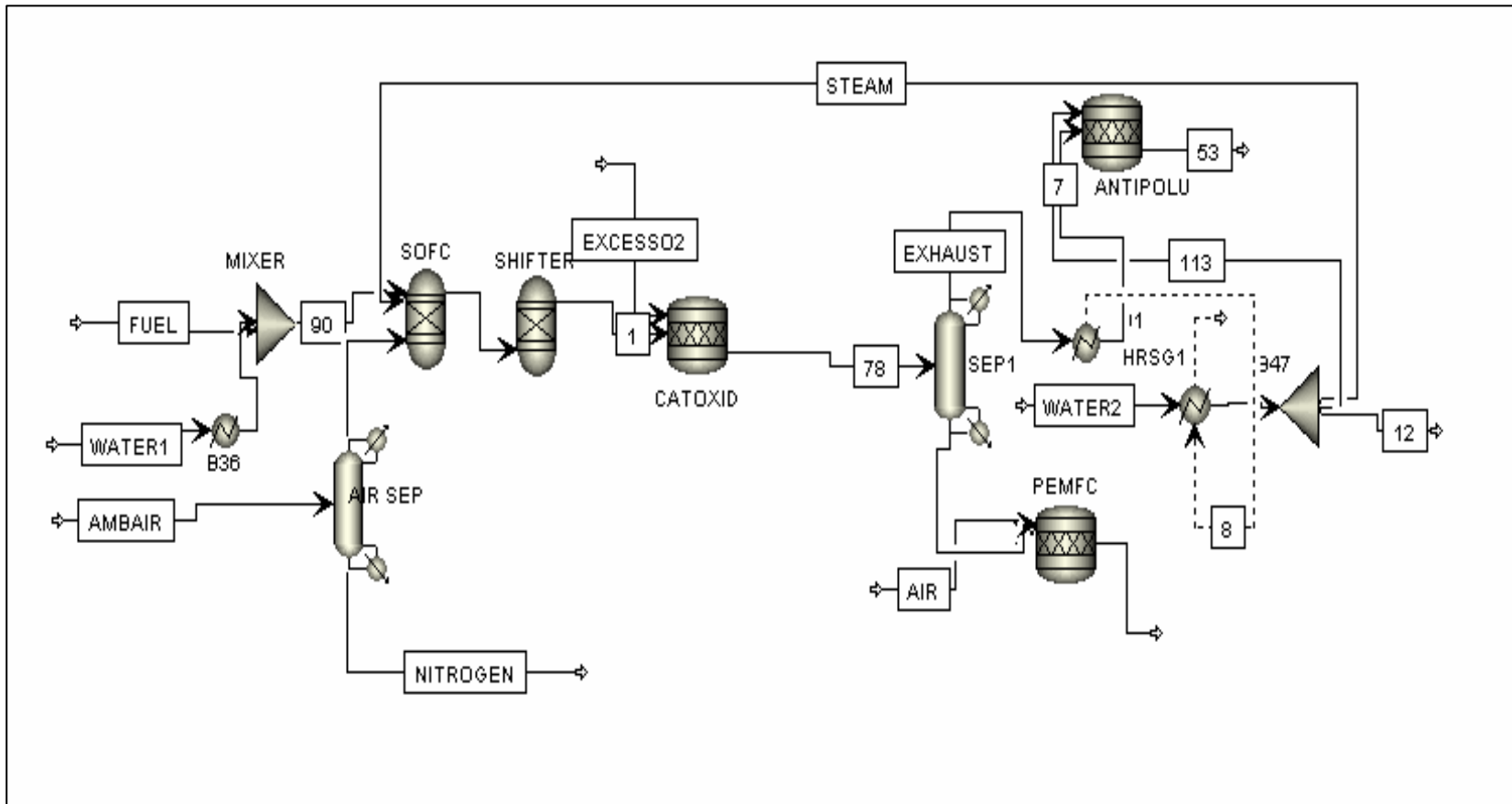


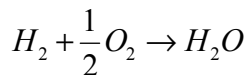
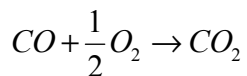
**Figure 1:** Aspen Plus flowsheet for SOFC-PEMFC hybrid power plant



**2.2 Solid Oxide and Proton Exchange Membrane Fuel Cell:** The old and new models used for the SOFC and PEMFC have been explained in detail in section 3.

**2.3 Low Temperature Shifter:** The exhaust from the SOFC contains carbon monoxide (CO) which is a poison for PEMFC electrodes. Hence it is passed over to a low temperature shifter which is modeled as a Gibbs reactor (SHIFTER) at 300 °F. The reactions occurring in the reactor decrease the CO in the stream from 8.13 to 0.022 lbmol/hr. But even this tiny amount of CO may adversely affect PEMFC performance. Hence this stream is passed over to a selective catalytic oxidizer to completely remove the CO.

**2.4 Selective Catalytic Oxidizer:** This module reduces the CO in the stream to below 10 ppm. This component is modeled by a stoichiometric reactor (CATOXID) with 10% excess oxygen. The two reactions occurring in the oxidizer are:



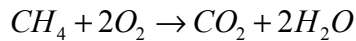
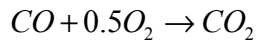
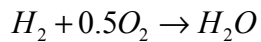
The fractional conversion for CO is specified as '1' since CO has to be eliminated completely and fractional conversion for O<sub>2</sub> in reaction 2 is also specified as '1'. The exhaust from CATOXID is at a high temperature of 1750 F and contains 50% by wt. of H<sub>2</sub>O and 25% by wt. of hydrogen (H<sub>2</sub>). The stream is separated into pure H<sub>2</sub> and the rest, by a separator SEP1. The pure H<sub>2</sub> stream is passed to the PEMFC and the other steam is transferred to a heat recovery steam generator (HRSG) which converts water to steam.

**2.5 Heat Recovery Steam Generator(HRSG):** The exhaust from the SEP1 is at a temperature of around 1750 F. The heat of this exhaust is used to convert 10 lbmol/hr of water to steam with a HRSG modeled by heater HRSG1. When the exhaust is cooled, 187000 Btu/hr of heat is extracted which is used to convert the water to steam. A part of this steam is recycled back to the SOFC where it is used as a reactant for the reforming reactions and downstream shift reactions, and to control against carbon deposition.

Finally, the exhaust from heater "B1" contains small amounts of pollutants like CO, H<sub>2</sub> and moderate amounts of methane (CH<sub>4</sub>). These are converted to carbon dioxide (CO<sub>2</sub>) and water (H<sub>2</sub>O) in a stoichiometric reactor (ANTIPOLU) with the following reactions in which fractional conversions for CO, H<sub>2</sub> and CH<sub>4</sub> are specified as '1'.

Power Rating	1472 kW	<b>Overall Efficiency</b>	72.6%
<b>Capital Cost</b>	1773 \$/kW	<b>CO<sub>2</sub> Emissions</b>	0.271 kg/kWh
<b>Cost of Electricity</b>	6.35 c/kWh		
SOFC		PEMFC	
Temperature	1750 °F	Temperature	176 °F
Pressure	20 psi	Pressure	25 psi
<b>Current Density</b>	75 mA/cm <sup>2</sup>	<b>Current Density</b>	190 mA/cm <sup>2</sup>
Fuel Utilization	70%		
Equivalence Ratio	1.25		

**Table 1:** Design and performance results for the hybrid power plant using the old fuel cell models



The key assumptions in this advanced flowsheet model are: (1) staged cells can be manufactured and installed at the same cost as unstaged cells, and (2) a sufficient number of cells can be staged so as to closely approach the limiting case performance for staged cells. Design and performance results for the hybrid power plant simulated in Aspen Plus using the old SOFC and PEMFC models are summarized in table 1.

### **3. Reducing uncertainties in the fuel cell models**

The main goal of this work is to reduce the uncertainties in the multi-objective design of the SOFC-PEMFC hybrid power plant by utilizing higher order models for both the fuel cells and thereby identify the optimal model complexity to enable simulation of the plant with satisfactory accuracy. As a first step, this section presents an overview of the old and new models of both types of fuel cells and identifies the main areas of improvement.

### 3.1 Solid oxide fuel cells (SOFC)

The basic physical structure or building block of a fuel cell consists of an electrolyte layer in contact with a porous anode and cathode on either side. The fuel or oxidant gases flow past the surface of the anode or cathode opposite the electrolyte and generate electrical energy by the electrochemical oxidation of fuel, usually hydrogen, and the electrochemical reduction of the oxidant, usually oxygen. The electrolyte not only transports dissolved reactants to the electrode, but also conducts ionic charge between the electrodes and thereby completes the cell electric circuit. The functions of porous electrodes in fuel cells are to provide a surface site where gas/liquid ionization can take place and to conduct ions away from interface once they are formed. As with batteries, individual fuel cells must be combined to produce appreciable power levels and so are joined in series by interconnects in a stack. Interconnects must be electrical conductors and impermeable to gases. Figure 2 shows a schematic configuration of a planar SOFC.

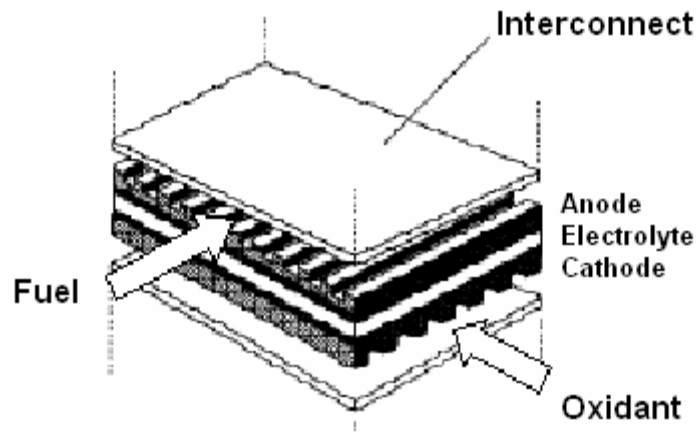
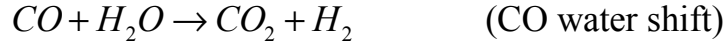


**Figure 2:** Fuel cell repeated unit in a fuel cell stack.

Since Aspen Plus [4, 5] does not include any inbuilt fuel cell model, there are two approaches to overcome this problem. The first way is to use a standard reactor model, like a stoichiometric and/or equilibrium reactor, to perform energy and mass balances around the fuel cell. This unit is then coupled with a polarization model for voltage and current computations. Alternatively, a new unit (User Model) based on a FORTRAN subroutine is used to perform mass and energy balances and polarization characterization. The former approach has been chosen for both the old and new SOFC models. The unit operation blocks used for both models are similar. As seen in figure 1, 20 lbmol/hr of natural gas fuel (FUEL) and 20 lbmol/hr of H<sub>2</sub>O (WATER1) are mixed and sent to the SOFC modeled using an 'RGIBBS' equilibrium reactor module which computes chemical equilibrium based on Gibbs free-energy minimization. The difference lies in the FORTRAN subroutine to calculate the current density – voltage characteristics and the total cell area.

The reactions that take place in a fuel cell are: methane steam reforming, carbon monoxide water shift and hydrogen electrochemical oxidation.



The first two reactions are at equilibrium [6] while hydrogen oxidation has fixed extent in order to match the given fuel utilization. Fuel utilization is defined as:

$$U_f = \frac{H_2^{reacted}}{4CH_4^{in} + CO^{in} + H_2^{in}} \quad (3.1)$$

where  $H_2^{reacted}$  are the total moles of hydrogen reacted,  $CH_4^{in}$ ,  $CO^{in}$ ,  $H_2^{in}$  are the moles of methane, carbon monoxide and hydrogen entering the cell respectively, 4 moles of  $H_2$  are generated by each mole of methane and so  $CH_4^{in}$  is multiplied by 4 and analogously  $CO^{in}$  is multiplied by 1.

The reaction extent of the electrochemical reaction is determined by a “design specification” that acts as a feedback controller. Reaction extent is manipulated so that:

$$O_2^{in} - O_2^{out} = \frac{1}{2} \cdot U_f \cdot (4CH_4^{in} + CO^{in} + H_2^{in}) \quad (3.2)$$

where  $O_2^{in}$  and  $O_2^{out}$  are the moles of oxygen entering and exiting the cell and  $U_f$  is the fuel utilization. Oxygen was chosen as the reference element because it reacts only with hydrogen. Recycling of the gaseous outlet of the cell is necessary in order to reach the desired fuel conversion. The electrochemical oxidation of CO was neglected because in presence of water, the favorable path for the oxidation of carbon monoxide is generating hydrogen by the water shift reaction [6, 7].

At a fixed temperature, a heat balance around the reactor gives the power output ‘ $hd$ ’ of the cell. The power output divided by the current (known once the fuel utilization is fixed) gives the voltage of the cell. Current can be computed as

$$ISOFC = 2 \cdot F \cdot H_2^{reacted} = 2 \cdot F \cdot U_f \cdot (4CH_4^{in} + CO^{in} + H_2^{in}) \quad (3.3)$$

where  $ISOFC$  is the current (A) and  $F$  is the Faraday constant (96485 C/mol). At this point, an SOFC polarization model is used to compute the current density of the cell at that given voltage.

### 3.1.1 Old SOFC polarization model

The polarization model used in our earlier studies is based on the work by Geisbrecht [8] and is described below. The SOFC current density is given by:

$$cdsofc = cdim \left( \frac{eref - ecell}{r} \right) (2.54 * 12)^2 \quad (3.4)$$

'*cdsofc*' is the SOFC current density (in mA/cm<sup>2</sup>)

'*cdim*' is the ratio of the mean current density to the minimum current density of SOFC calculated iteratively within the process flowsheet and given by the equation:

$$cdim = \left\{ \frac{\left( \int_{X_r} \frac{eref - ecell}{eloc - ecell} dX \right)^{-1}}{X_r} \right\} \quad (3.5)$$

'*eref*' is the reference Nernst potential (in V)

'*ecell*' is the operating cell voltage (in V) given by:

$$ecell = \frac{(1000 * \frac{hd}{3412})}{ISOFC} \quad (3.6)$$

'*hd*' is the heat duty of the RGIBBS reactor representing the SOFC (Btu/hr)

'*ISOFC*' is the current in the SOFC (in A)

'*3412*' is the conversion of the heat duty is Btu/hr to kilowatt-hour

'*1000*' is the conversion of kilograms to grams consistent with the units of ISOFC

'*eloc*' is the local nernst potential (in V)

'*X<sub>r</sub>*' is the reference fuel conversion

'*r*' is the cell ohmic resistance (0.73 ohm/cm<sup>2</sup>) taken from the fuel cell hand book [7]

After flowsheet convergence, a design sequence is executed one time to determine the current density distribution. Converged results (fuel and air feeds including recycle, fuel conversion, cell voltage and heat loss.) are used as input. An outer iteration is used to determine cell area, and an inner loop is used to cycle through the discretized cell. Calculation blocks are used to store fuel and air stream vectors and to determine current in each element that equilibrates the local Nernst potential to the cell voltage using cell area and local resistance [8].

This model does not take into factor any voltage losses due to: 1) activation polarization, 2) concentration polarization and 3) ohmic polarization. This induces a considerable degree of error in the prediction as will be shown in the results and discussion section. This necessitated selection of a higher level model for the SOFC. Selecting a suitable SOFC model to implement involved a survey of various models available in literature. There are number of papers in the literature concerning SOFC behavior modeling which could be classified as steady state [9-16] and dynamic [17] models. A 1-dimensional, steady state, algebraic polarization model derived from literature [11] was used for our study.

### 3.1.2 Higher level SOFC model

Equations 3.7-3.13 represent the main equations of the 1-dimensional, steady state, algebraic polarization model [11]. This particular model was chosen because of its simplicity and comprehensive nature (applicability to every operating condition and sensitivity to the various design components of the cell). Overpotential equations, based on the complete Butler-Volmer and diffusion equations, are obtained together with the necessary parameters from the reference [11].

$$E(cdsofc) = E_0 - \eta_{Ohm} - \eta_{Act,a} - \eta_{Act,c} - \eta_{Conc,a} - \eta_{Conc,c} \quad (3.7)$$

$$E_0 = \frac{\bar{RT}}{2F} \ln K - \frac{\bar{RT}}{4F} \ln \left( \frac{(p_{H_2O}^I)^2 p_0}{(p_{H_2}^I)^2 p_{O_2}^I} \right) \quad (3.8)$$

$$\eta_{Ohm} = cdsofc \times R_e \quad (3.9)$$

$$\eta_{Act,a} = \frac{2\bar{RT}}{n_e F} \sinh^{-1} \left( \frac{cdsofc}{2 \times cdsofc_{0a}} \right) \quad (3.10)$$

$$\eta_{Act,c} = \frac{2\bar{RT}}{n_e F} \sinh^{-1} \left( \frac{cdsofc}{2 \times cdsofc_{0c}} \right) \quad (3.11)$$

$$\eta_{Conc,a} = -\frac{\bar{RT}}{2F} \ln \left( \frac{(1 - (\bar{RT}/2F)(l_a / D_{a(eff)}) p_{H_2}^I) cdsofc}{(1 + (\bar{RT}/2F)(l_a / D_{a(eff)}) p_{H_2O}^I) cdsofc} \right) \quad (3.12)$$

$$\eta_{Conc,c} = -\frac{\bar{RT}}{4F} \ln \left[ \frac{(p_c / \delta_{O_2}) - ((p_c / \delta_{O_2}) - p_{O_2}^I) \exp[(\bar{RT}/4F)(\delta_{O_2} l_c / D_{c(eff)}) p_c] cdsofc}{p_{O_2}^I} \right] \quad (3.13)$$

Where:

$cdsofc$  = current density (A/m<sup>2</sup>)

$E(cdsofc)$  = Cell voltage as a fn. of current density (V)

$E_0$  = Ideal cell voltage without any losses (V);

$\eta_{Ohm}$  = Ohmic Polarization (V)

$\eta_{Act,a}$  = Anodic activation polarization (V)

$\eta_{Act,c}$  = Cathodic activation polarization (V)

$\eta_{Conc,a}$  = Anodic concentration polarization (V)  
 $\eta_{Conc,c}$  = Cathodic concentration polarization (V)  
 $R_e$  = Electrolyte area-specific ohmic resistance ( $\Omega /m^2$ )  
 $\bar{R}$  = Universal gas constant ( $=8.314Jmol^{-1}K^{-1}$ )  
 $T$  = Temperature (K)  
 $F$  = Faraday constant ( $=96485 C mol^{-1}$ )  
 $K$  = equilibrium constant  
 $p^I_{H_2O}$  = Partial pressure of  $H_2O$  in the inlet stream (Pa)  
 $p^I_{H_2}$  = Partial pressure of  $H_2$  in the inlet stream (Pa)  
 $p^I_{O_2}$  = Partial pressure of  $O_2$  in the inlet stream (Pa)  
 $\delta_{O_2}$  = ratio of Knudsen diffusion coefficients  
 $p_0$  = Atmospheric pressure (Pa)  
 $n_e$  = electrons transferred per reaction  
 $cdsofc_{0a}$  = anode exchange current density ( $Am^{-2}$ )  
 $cdsofc_{0c}$  = cathode exchange current density ( $Am^{-2}$ )  
 $l_a$  = anode thickness (m)  
 $D_{a(eff)}$  = effective diffusion coefficient (anode) ( $m^2s^{-1}$ )  
 $l_c$  = cathode thickness (m)  
 $D_{c(eff)}$  = effective diffusion coefficient (cathode) ( $m^2s^{-1}$ )  
 $p_c$  = cathode pressure (Pa)

Since the model gives the voltage as a function of current density, Newton-Raphson method (3.15) is applied in order to get iteratively the current density at the desired voltage:

$$V(i) - \bar{V} = f(i) = 0 \quad (3.14)$$

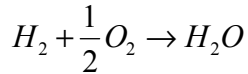
$$i_{n+1} = i_n - \alpha \cdot \frac{f(i)}{f'(i)} \quad (3.15)$$

where  $V(i)$  is the voltage as function of current density ( $i$ ),  $\bar{V}$  is the desired voltage,  $\alpha$  is a weight parameter, and  $f'(i)$  is the numerical derivative of  $f(i)$ .

Once the current density is obtained, current divided by current density gives the total cell area (area of the electrodes), important for cost estimations.

### **3.2 Proton Exchange Membrane fuel cell (PEMFC)**

The utilization of the reformed fuel is completed in the PEMFC where more favorable thermodynamics apply. 21.57 lbmol/hr of pure hydrogen enters the PEMFC modeled as a stoichiometric reactor (PEMFC) in figure 1. The reaction occurring in the reactor is specified as:



Here the fractional conversion of  $H_2$  is specified as '1' (implying 100% fuel utilization).

### 3.2.1 Old PEMFC model

The model methodology for the PEMFC is similar to that employed in the old SOFC model. A stoichiometric reactor performs energy and mass balances around the fuel cell. This unit is then coupled with a polarization model for voltage and current computations. The cell voltage as a function of the current density is defined by equations 3.16-3.18

$$E(cdpem) = E_0 - \eta_{act} - \eta_{conc} \quad (3.16)$$

$$\eta_{act} = 0.04249 + 0.030395 * \log(cdpem) \quad (3.17)$$

$$\eta_{conc} = -4.336 \times 10^{-5} \times T \times \log\left(1 - 0.001 * \frac{cdpem}{1.1}\right) \quad (3.18)$$

$cdpem$  = current density ( $A/cm^2$ ).

$E(cdpem)$  = Cell voltage as a function of current density (V)

$E_0$  = reference voltage (V)

$\eta_{act}$  = activation polarization (V)

$\eta_{conc}$  = concentration polarization (V)

$T$  = temperature of outlet stream from PEMFC (K)

The PEMFC model gives the voltage as a function of current density. Again, Newton-Raphson method (3.15) is applied in order to get iteratively the current at the desired voltage: The calculated current density is adapted to the cost model for the fuel cell using equation 3.21.

$$cd = cdimp * 0.001 * cdpem * (2.54 * 12)^2 \quad (3.21)$$

' $CD$ ' is the PEMFC current density (in  $mA/cm^2$ )

' $cdimp$ ' is the ratio of mean current density to the minimum current density of PEMFC calculated iteratively within the process flowsheet (analogous to equation 3.5)

' $cdpem$ ' is the value of current density in the PEMFC calculated iteratively as shown previously ( $A/cm^2$ ).

### 3.2.2 Higher Level PEMFC model

The new PEMFC model is based on the work of Maggio et al. [18]. Maggio et al. developed a one-dimensional steady state simulation model considering also electrode flooding and membrane dehydration, which is not accounted for in the old model. The irreversible losses (overpotentials) which make the cell voltage lower than the ideal theoretical value are computed as a function of operating conditions, current density, membrane properties, catalyst



properties, water management, and empirical parameters. The dependence on so many parameters makes the model suitable for different cell conditions and designs, unlike purely empirical models which are tuned on one particular case. The main equations for the model are provided in equations 3.22 – 3.30. Some salient points of the model are:

- Cell resistance is considered to vary as a function of the current density, depending on the water balance conditions.
- Unlike classical approaches, the limiting current density ( $i_{lim}$ ) varies as a function of the cell current density.
- Gas porosity in the diffusional layer depends on current density.
- Membrane ionic conductivity varies according to the anode or cathode dehydration.

$$E(cdpem) = E_0 - \eta_{act} - \eta_{ohm} - \eta_{dif} - \eta_{conv} \quad (3.22)$$

$$E_0 = 1.23 - 0.9 \times 10^{-3} (T - 298) + \frac{\bar{R}T}{4F} \ln(p_{H_2}^2 p_{O_2}) \quad (3.23)$$

$$\eta_{act} = \frac{RT}{F} \ln\left(\frac{cdpem}{cdpem_0}\right) \quad (3.24)$$

$$\eta_{ohm} = cdpem \times R_{cell} \quad (3.25)$$

$$\eta_{dif} = \omega T I \ln\left(\frac{cdpem_{lim}}{cdpem_{lim} - 1}\right) \quad (3.26)$$

$$\eta_{conv} = F c_{H^+} v \frac{l_m}{\kappa} \quad (3.27)$$

$$cdpem_0 = cdpem_{0,Pt} S_{Pt} W_{Pt} U_{Pt} \quad (3.28)$$

$$R_{cell} = \frac{l_m}{\kappa \tau_R} \quad (3.29)$$

$$cdpem_{lim} = -\frac{2FD_{O_2N_2} (\epsilon_g^d)^{1.5} (T / 273)^{0.823}}{V_m l_{d+}} \ln(1 - x_{O_2}) \quad (3.30)$$

Where:

$E_0$  = open circuit voltage

$\eta_{act}$  = activation overpotential

$\eta_{ohm}$  = ohmic overpotential

$\eta_{dif}$  = diffusion overpotential

$\eta_{conv}$  = overpotential associated with proton transport for convection

$\bar{R}$  = Universal gas constant (=8.314 J mol<sup>-1</sup> K<sup>-1</sup>)

T = Temperature (K)

F = Faraday constant (=96485 C mol<sup>-1</sup>)

$cdpem$  = current density (A cm<sup>-2</sup>)

$cd_{pem_0}$  = exchange current density ( $Acm^{-2}$ )  
 $R_{cell}$  = cell resistance ( $\Omega cm^2$ )  
 $\omega$  = empirical constant for diffusion overpotential ( $\Omega cm^2 K^{-1}$ )  
 $cd_{pem_{lim}}$  = limiting current density ( $Acm^{-2}$ )  
 $c_{H^+}$  = fixed charge concentration ( $molcm^{-3}$ )  
 $l_m$  = wet membrane thickness (cm)  
 $v$  = water velocity in membrane pores ( $cms^{-1}$ )  
 $\kappa$  = membrane ionic conductivity ( $\Omega^{-1}cm^{-1}$ )  
 $cd_{pem_{0,Pt}}$  = exchange current density per Pt surface ( $Acm^{-2}Pt$ )  
 $S_{Pt}$  = Catalyst surface area ( $cm^2mg^{-1}$ )  
 $W_{Pt}$  = catalyst loading ( $mgcm^{-2}$ )  
 $U_{Pt}$  = catalyst utilization  
 $\tau_R$  = membrane resistance/cell resistance ratio  
 $D_{O_2N_2}$  = oxygen/nitrogen binary diffusion coefficient at standard conditions ( $cm^2s^{-1}$ )  
 $\epsilon_g^d$  = gas porosity in gas-diffusion layer  
 $V_m$  = standard molar volume ( $22414 cm^3mol^{-1}$ )  
 $l_{d+}$  = cathode gas-diffusion layer thickness (cm)  
 $x_{O_2}$  = gas-phase mole fraction of  $O_2$

#### **4. Multi-objective optimization framework and Uncertainty Analysis**

It has been shown in our earlier work [3] that this SOFC-PEMFC hybrid power plant poses a multi-objective problem. Table 2 shows the multi-objective optimization problem formulation for this SOFC-PEMFC hybrid power plant.

<b>Objectives :</b>	<i>Subject to</i>
	<ul style="list-style-type: none"> <li>✓ <i>Mass &amp; energy balance constraints</i></li> <li>✓ <i>Power rating of 1472 kW (Base case)</i></li> </ul>
<ul style="list-style-type: none"> <li>✓ Min Capital cost (CAP)</li> <li>✓ Min Cost of electricity (COE)</li> <li>✓ Min CO<sub>2</sub> emissions (CO2EM)</li> <li>✓ Max Current density SOFC (CDSOFC)</li> <li>✓ Max Current density PEM (CDPEM)</li> <li>✓ Max Overall efficiency (ACEFF)</li> </ul>	<i>Decision variables</i> <ul style="list-style-type: none"> <li>✓ <i>Fuel utilization (UTIL)</i></li> <li>✓ <i>Equivalence ratio (ERAT)</i></li> <li>✓ <i>Pressure of the PEM (PPEM)</i></li> <li>✓ <i>Fuel Flow (FUEL)</i></li> <li>✓ <i>Air Flow (AIR)</i></li> </ul>

**Table 2:** The objectives, constraints and decision variables for the SOFC-PEM hybrid fuel cell power plant

As is well known, mathematics cannot isolate a unique optimum when there are multiple competing objectives. Mathematics can at most aid designers to eliminate design alternatives dominated by others, leaving a number of alternatives in what is called the Pareto set. For each of these solution alternatives, it is impossible to improve one objective without sacrificing the value of another one. In our earlier work [3], we computed the Pareto set for this multi-objective problem using the old models of SOFC and PEMFC. However, as mentioned earlier, these models have significant uncertainties in them. As a first step towards analyzing the effect of uncertainties, we used the experimental data from [8] to characterize and quantify uncertainties. It was found that the Pareto surfaces obtained using deterministic and stochastic analysis, were significantly different [3]. In this work, we are extending this analysis further. As better experimental data is available, we re-characterized the uncertainties in old as well new models using this new experimental data from the literature [18, 19]. Pareto surfaces are generated for the old and new deterministic and stochastic models. The aim is to find the optimal model complexity for such an analysis.

#### **4.1 Characterization and quantification of uncertainty**

The uncertainty analysis consists of 4 main steps: (1) characterization and quantification of uncertainty in terms of probability distributions, (2) sampling from these distributions, (3) propagation through the modeling framework, (4) analysis of results [20]. The first step is of foremost importance on which the validity of the uncertainty analysis rests on. Characterization refers to the process of representing uncertainty through mathematical expressions in order to facilitate analysis with mathematical tools [21]. In this case, the uncertainties in the fuel cell models have been quantified in terms of a parameter called the “Uncertainty Factor” (UF) defined as the ratio between the model predicted voltage and the experimental voltage for each current density. Quantification refers to the representation of uncertainty with probability distribution functions (PDF) illustrating the frequency of occurrence of each uncertainty. In uncertainty analysis, the output variables like the different objective function values which are functions of the uncertain parameters do not have a specific point value. In our analysis, they are represented as expected values over repeated sampling iterations. The probability distributions of each uncertain parameter are sampled and propagated through the framework and this is repeated a specific number of times to compute the expected value of the objectives. The sampling technique employed also has an impact on efficiency of the uncertainty analysis. This is discussed in the next sub-section. Figures 3 and 4 show the uncertainty distributions of the new and old SOFC models.

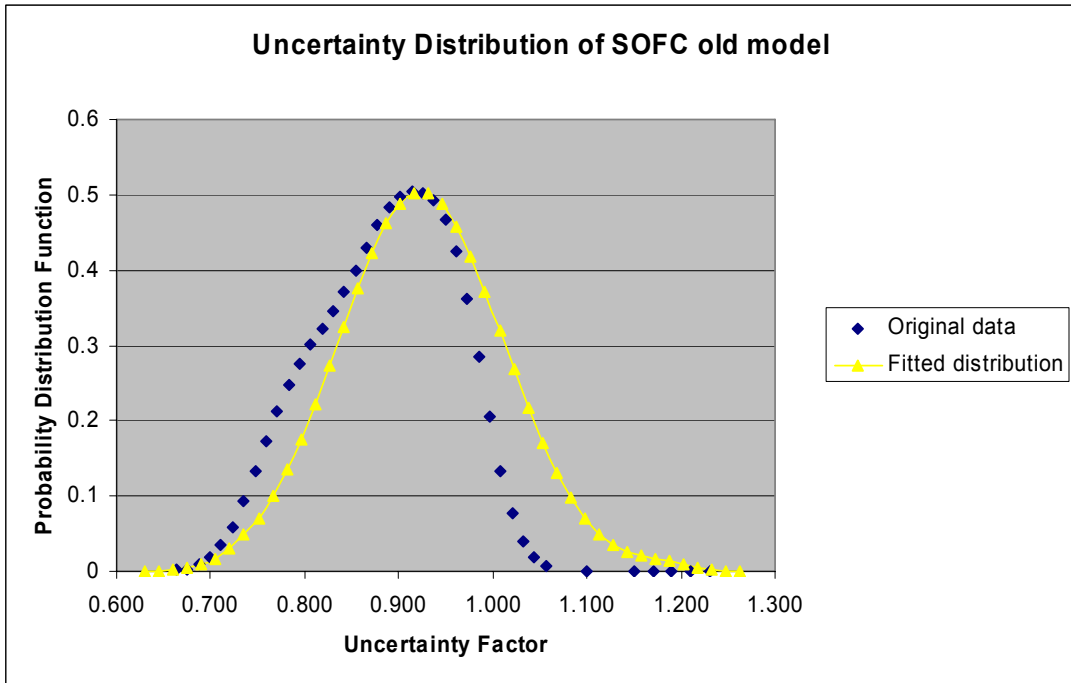


**Figure 3:** Uncertainty distribution of UF for the SOFC old model

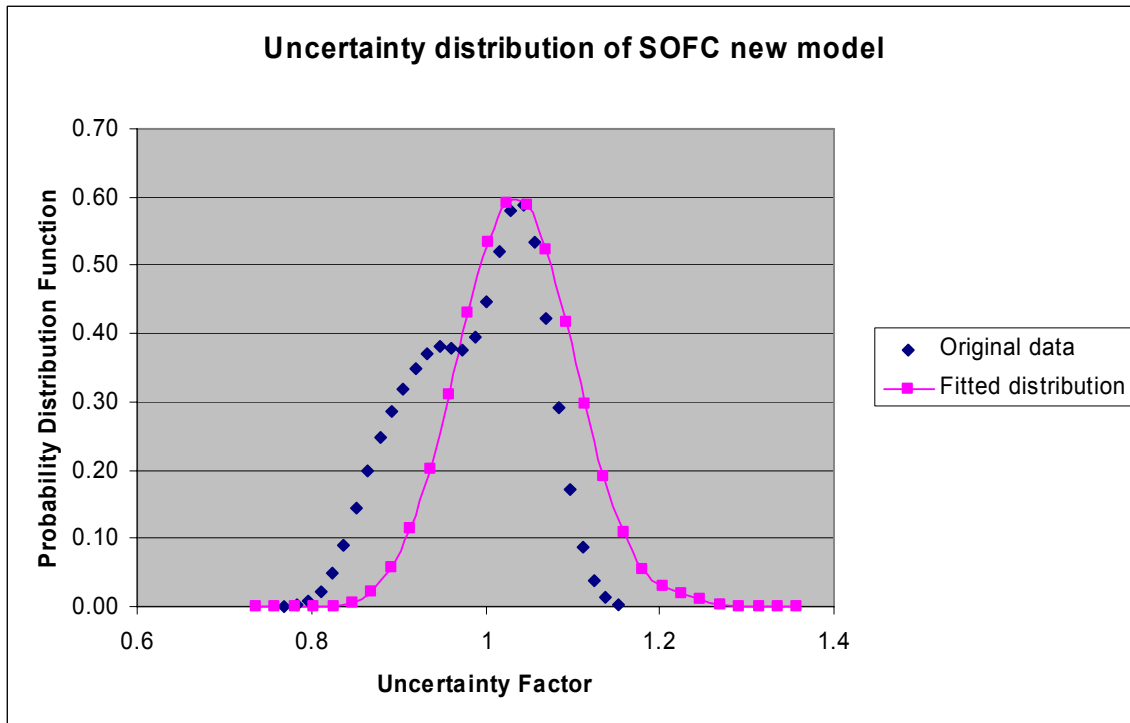


**Figure 4:** Uncertainty distribution of UF for the SOFC new model

The figures illustrate the reduction of uncertainty facilitated by the higher level SOFC model. The variance of the uncertainty distribution has decreased in figure 4 and additionally, the most likely value (mean) is very close to 1 which means that the model predicted voltage values are closer to the experimental voltages for all current densities compared to the mean of the uncertainty distribution for the old model which is around 0.9. Similarly, figures 5 and 6 illustrate the comparison between the levels of uncertainty in the new and old PEMFC models respectively.

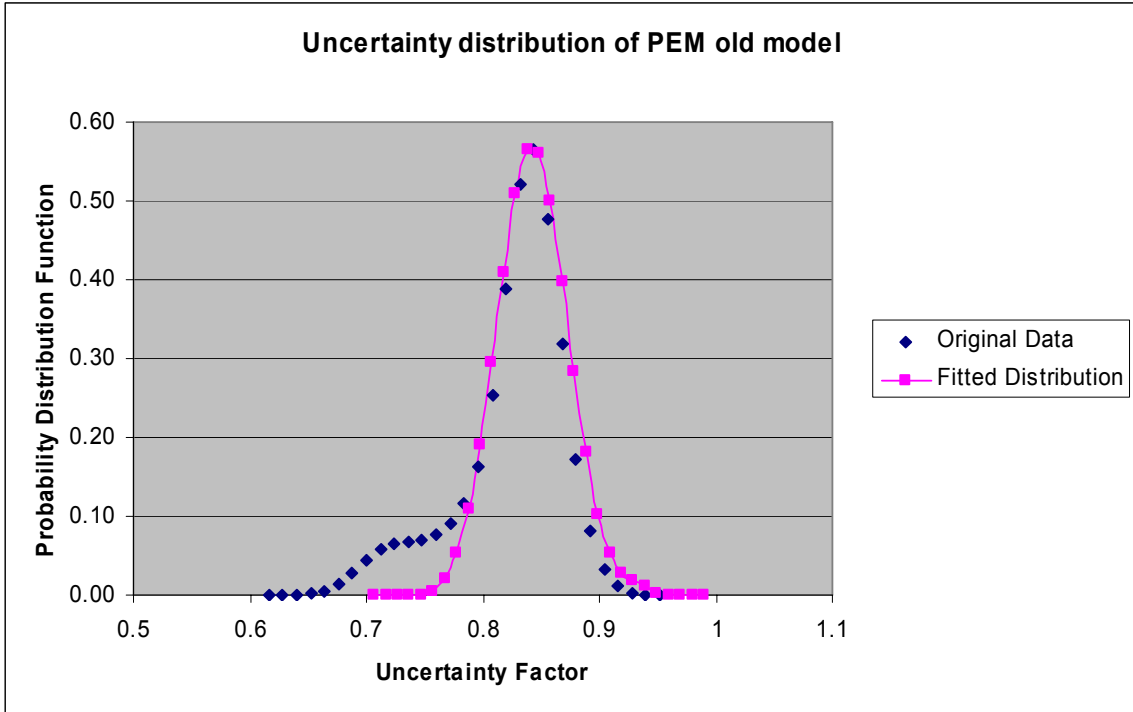


**Figure 5:** Uncertainty distribution of UF for PEMFC old model

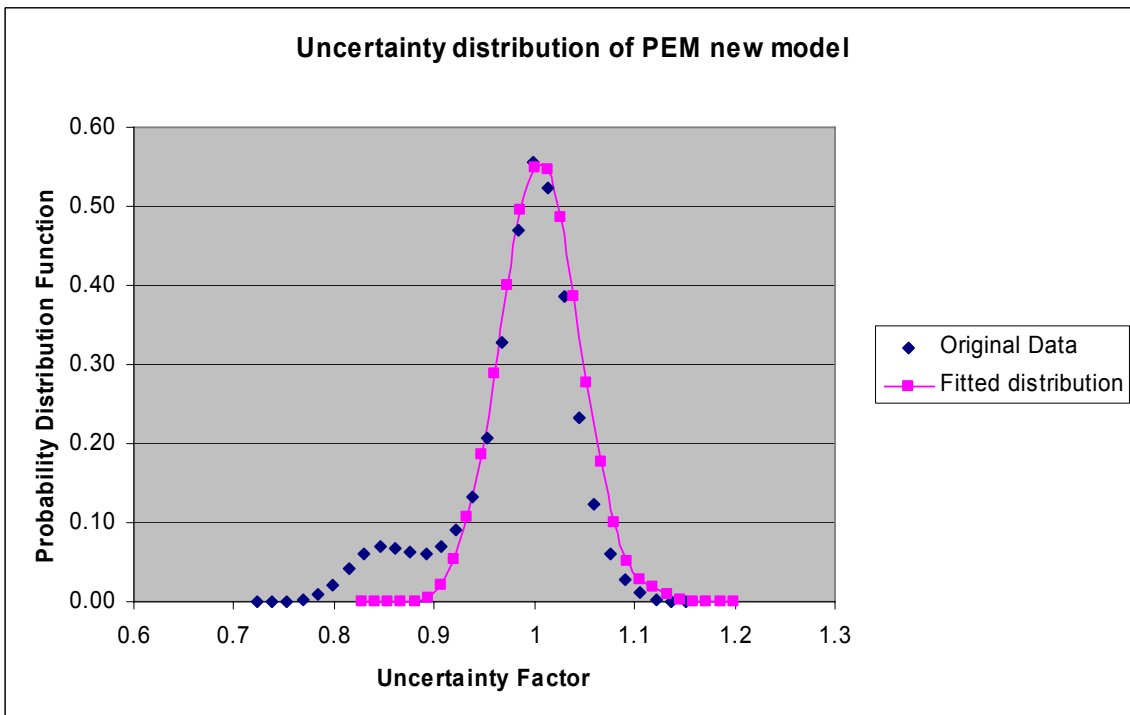


**Figure 6:** Uncertainty distribution of UF for PEMFC new model

An interesting point to note in the case of PEMFC, is that though there is no difference between the variance of the two plots, the most likely value (and mean) of the uncertainty distribution plot for the new PEMFC model is almost equal to 1, while that for the old model is 0.83. This means that, there is little reduction of uncertainty between the old and new model, but the new model is considerably much more accurate than the old model.

#### 4.2 Pareto Surface computation and analysis

The next step is to sample the distributions, propagate the uncertainties and obtain stochastic multi-objective optimization trade-off surfaces. The conceptual framework for this stochastic MOP problem is shown in figure 7, where the outer multi-objective optimization algorithm is used to formulate number of optimization problems to generate the Pareto set of non-dominating alternatives. The inner most loop addresses the question of uncertainty where the deterministic model is converted to stochastic model. Both these loops are recursive and computationally very expensive as compared to a single deterministic optimization problem. Therefore, we utilize efficient algorithms to alleviate this problem.

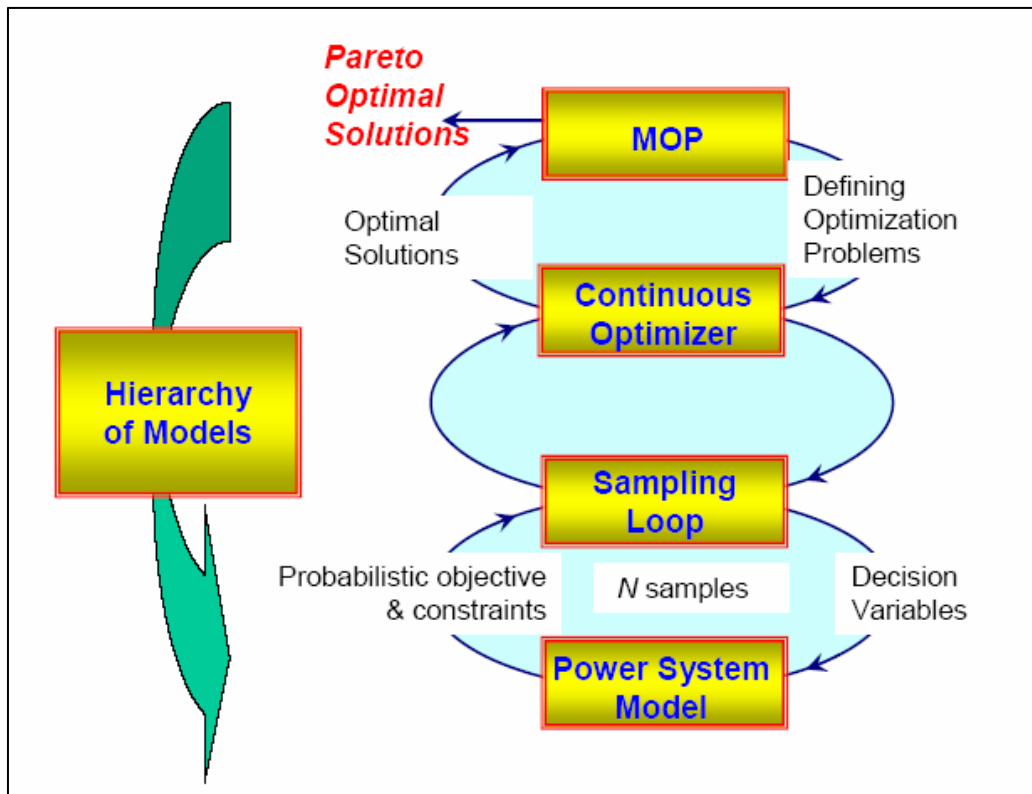


**Figure 7:** The algorithmic framework for MOP under uncertainty with hierarchy of models.

A generalized Multi-objective(MOP) problem can be formulated as follows:

$$\begin{aligned} \min \quad & Z = Z_i, i = 1, \dots, p, \quad p \geq 2 \quad (3.31) \\ \text{s.t.} \quad & h(x, y) = 0, \\ & g(x, y) \leq 0, \end{aligned}$$

where  $x$  and  $y$  are continuous like flowrate, design variables, and discrete decision variables related to type of fuel, selection of units, connectivity of units in the flowsheet, and  $p$  is the number of objective functions. The functions  $h(x, y)$  and  $g(x, y)$  represent the equality and inequality constraints, respectively. There is a large array of analytical techniques to solve this MOP problem; however, the MOP methods are generally divided into two basic types: preference-based methods and generating methods [2]. Preference-based methods like goal programming attempt to quantify the decision-maker's preference, and with this information, the solution that best satisfies the decision-makers' preference is then identified. Generating methods, such as the weighting method and the constraint method, have been developed to find the exact Pareto set or an approximation of it. In this work, it is necessary to develop appropriate multi-criteria techniques to provide decision makers with the complete economic environmental-operational surface, so that decision makers would know the full range of alternatives and understand the trade-offs among the objectives implied by each alternative before making their selection. This involves finding a population of solutions from a very large number of design alternatives, such that no one dominates any of the others in the population (generating method). A pure algorithmic approach to solving is to select one of the objectives to minimize while the remaining others are turned into an inequality constraint with a parametric right-hand-side,  $L_k$ . The problem takes on the following form:

$$\begin{aligned} \min \quad & Z_j, \quad (3.32) \\ \text{s.t.} \quad & h(x, y) = 0, \\ & g(x, y) \leq 0, \\ & Z_k \leq L_k, k = 1, \dots, j-1, j+1, \dots, p, \end{aligned}$$

where  $Z_j$  is the chosen  $j$ -th objective that we wish to optimize. Solving repeatedly for different values of  $L_k$  leads to the Pareto set, and this approach is equivalent to calculating an integral over the space of objectives. For MOP under uncertainty, this problem includes probabilistic distributions for uncertain variables and the objective and constraints are expressed in terms of probabilistic functions like mean, variance, and fractiles. The MOP framework proposed in this work (Figure 7) involves three levels. Detailed descriptions and the proposed efficiency improvements of this framework are explained in the following paragraphs.

**Level 1, Sampling loop:** One of the most widely used techniques for sampling from a probability distribution is the Monte Carlo sampling technique, which is based on a pseudo-random generator to approximate a uniform distribution (i.e.,

having equal probability in the range from 0 to 1). The specific values for each input variable are selected by inverse transformation over the cumulative probability distribution. A Monte Carlo sampling technique also has the important property that the successive points in the sample are independent. Nevertheless, in most applications, the actual relationship between successive points in a sample has no physical significance; hence, the randomness/independence for approximating a uniform distribution is not critical. In such cases, uniformity properties plays a more critical role in sampling, as a result, constrained or stratified sampling techniques are more appealing. In recent years, efficient sampling techniques like Hammersley sequence sampling (HSS), and Latin Hypercube Hammersley Sampling (LHHS) based on Hammersley points has been proposed by our group [22, 23], which use an optimal design scheme for placing the  $n$  points on a  $k$ -dimensional hypercube. This scheme ensures that the sample set is more representative of the population, showing uniformity properties in multi-dimensions, unlike Monte Carlo, Latin hypercube [2], and its variant, the Median Latin hypercube sampling technique. It has been found that the HSS/LHHS techniques are at least 3 to 100 times faster than LHS and Monte Carlo techniques and hence is a preferred technique for uncertainty analysis, as well as nonlinear optimization under uncertainty.

**Level 2, Continuous optimizer:** This level deals with finding optimal decisions based on Non-Linear Programming (NLP) algorithms Among the quasi-Newton-based methods, the successive quadratic programming (SQP) method is used for this framework because it requires far fewer function and gradient evaluations than other methods for highly nonlinear constrained optimization, and it does not need feasible points at intermediate iterations. Both of these properties make SQP one of the most promising techniques for problems dealing with nonlinear constraint optimization, like process simulations.

**Level 3, MOP:** The multi-objective optimization algorithm used in this work is based on the newly developed MINSOOP algorithm [23]. This algorithm uses the HSS technique to generate combinations of the right-hand-side. The aim is to Minimize Number of Single Objective Optimization Problems (MINSOOP) by exploiting the  $n$ -dimensional uniformity of the HSS technique.

#### **4. Results and discussion**

The first step in computing the Pareto surface is calculation of the pay-off table, obtained by performing the optimization (maximization and minimization) for each objective individually without any constraints thereby obtaining the bounds for each objective. Tables 3 and 4 are the pay-off tables for the deterministic old MOP and stochastic old MOP respectively. The pay-off table is a first approximation to the trade-off surface and provides an overview of the trends for the designs. These two tables give an indication of the considerable differences between the stochastic and deterministic old model designs. Comparing corresponding designs in tables 3 and 4, it can be noted that the optimal decision variables for almost all of the designs are quite different and consequently, the objectives also vary. On the other hand, tables 5 and 6 show the degree of closeness between corresponding designs of the stochastic and deterministic



new model cases respectively. It can be clearly noted that most of the designs in tables 5 and 6 are appreciably close to each other except the maximum SOFC current density design. This can be attributed to the existence of multiple solutions due to the highly non-convex nature of the surface. Figure 8 illustrates the trade-offs for the deterministic and stochastic old model MOP respectively. Confirming the trends inferred from the pay-off tables, it can be seen that there is a considerable difference in the contour shape and levels between the Pareto surfaces; the deterministic MOP has underestimated the capital cost for a majority of the designs. Uncertainty analysis has introduced a marked change on the final trade-offs which leads us to the conclusion that the previous models utilized for the PEMFC and the SOFC have a higher degree of inaccuracy in predicting the fuel cell performances and reinforces the necessity for more accurate models of a higher complexity.

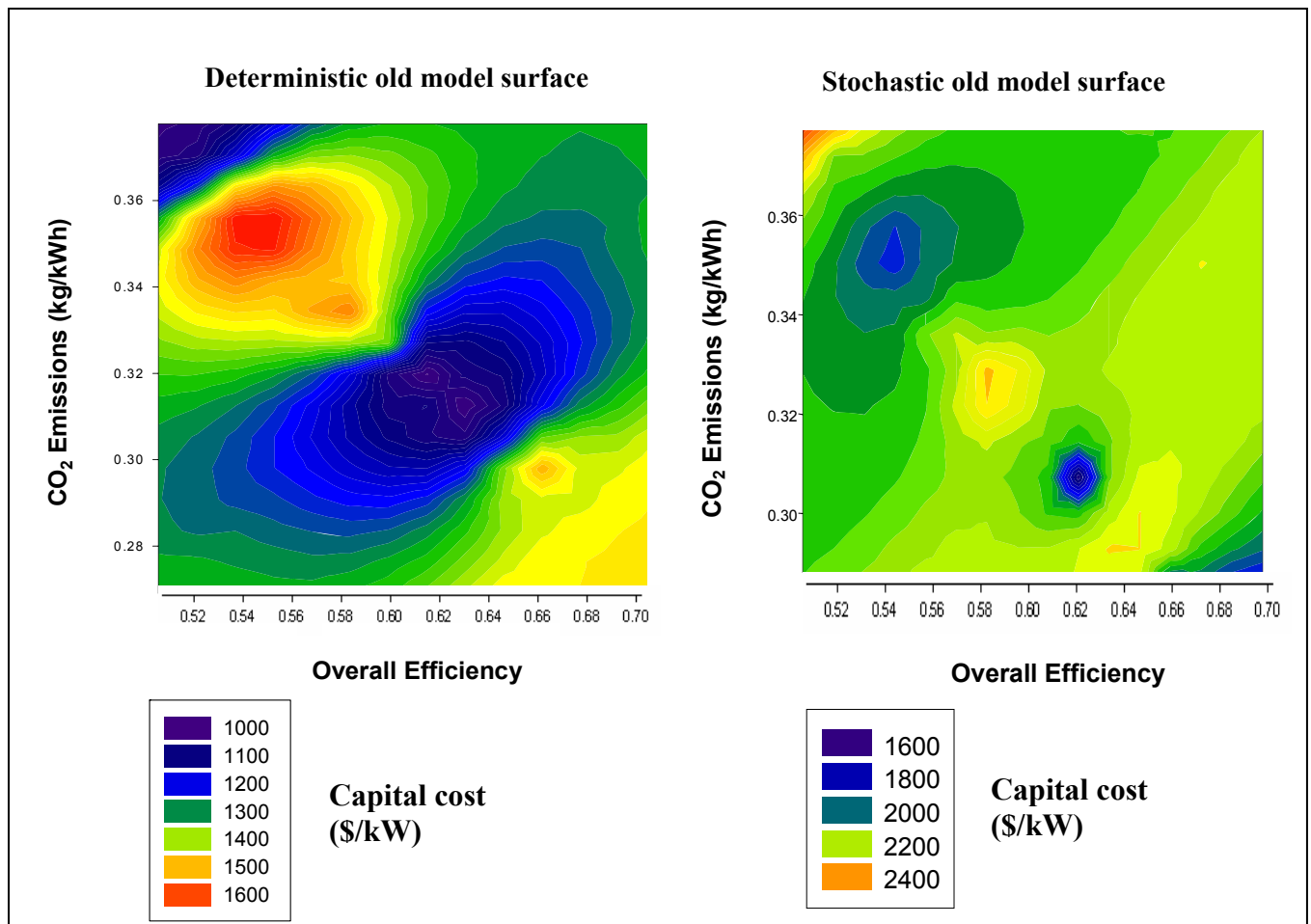


**Figure 8:** Comparison of the old model deterministic and old model stochastic MOP trade-off surfaces

	MAX	MIN	MIN	MIN	MAX	MIN	MAX	MIN	MIN	MAX
	ACEFF	ACEFF	CAP	COE	CO2EM	CO2EM	CDPEM	CDPEM	CDSOFC	CDSOFC
Design No.	1	2	3	4	5	6	7	8	9	10
<b>PWRTG</b>	1475.1856	1465.51	1568.3258 7	1469.0955	1634.2934 05	1470.4051	1500.2414 2	1496.3793	1471.963	1471.99
<b>ACEFF</b>	0.7232446	0.52	0.6008321	0.58273	0.5426174	0.7066749	0.5753043 7	0.7077066	0.7262587 77	0.5184094 19
<b>CAP</b>	1456.4933	1599.8093 8	994.78357 9	993.38655	1444.397	1281.9228 6	739.9451	1289.6887	1664.6514	563.50817 08
<b>COE</b>	5.67E-02	5.63E-02	4.16E-02	4.28E-02	5.05E-02	4.15E-02	3.68E-02	5.15E-02	6.28E-02	3.33E-02
<b>CO2EM</b>	0.2728659	0.3788568 4	0.3284591	0.3386584	0.3636978 4	0.2793638	0.343033	0.2788567 9	0.2717334	0.3806813 45
<b>CDSOFC</b>	101.86	672.009	531.131	616.0684	737.20968 9	157.61178 44	678.179	149.0192	76.34382	873.91427 17
<b>CDPEM</b>	290.3345	304.847	308.62476	307.62895	294.63637	294.38629	319.5917	287.22287	293.60287 6	318.95470 32
<b>UTIL</b>	0.69993	0.55147	0.43617	0.40266	0.41114	0.7	0.4	0.7	0.7	0.4039
<b>PPEM</b>	23.3115	36.8556	39.7391	36.189	20.1208	26.3631	75	20	25.3265	72.12
<b>ERAT</b>	1.37434	5.69168	1.25	1.25	3.01218	1.79611	1.88651	1.70141	1.25	4.566
<b>FUEL</b>	20.1683	27.8188	25.8102	24.9279	29.7814	20.5743	25.7853	20.9073	20.0408	28.07
<b>AIR</b>	189.276	851.883	137.29	122.408	359.824	252.367	189.831	242.929	171.08	505.365

**Table 3:** The bounds for different objectives calculated by deterministic old model multi-objective optimization

	MAX	MIN	MIN	MIN	MAX	MIN	MAX	MIN	MIN	MAX
	ACEFF	ACEFF	CAP	COE	CO2EM	CO2EM	CDPEM	CDPEM	CDSOFC	CDSOFC
Design No.	1	2	3	4	5	6	7	8	9	10
<b>PWRTG</b>	1466.273	1471.865	1400.025	1471.638	1496.265	1471.738	1471.233	1472.000	1520.825	1472.265
<b>ACEFF</b>	0.728	0.485	0.660	0.665	0.510	0.731	0.564	0.723	0.695	0.510
<b>CAP</b>	2695.595	3137.087	1932.397	1946.113	6326.013	3122.307	1929.479	2381.998	2039.052	2752.956
<b>COE</b>	0.084	0.089	0.065	0.065	0.158	0.095	0.063	0.078	0.068	0.081
<b>CO2EM</b>	0.271	0.407	0.299	0.297	0.387	0.270	0.350	0.273	0.284	0.387
<b>CDSOFC</b>	89.278	838.060	224.132	242.574	833.968	64.362	669.148	75.412	117.201	839.433
<b>CDPEM</b>	48.500	45.497	47.017	48.570	51.782	48.478	52.591	41.911	45.592	48.011
<b>UTIL</b>	0.697	0.450	0.580	0.628	0.427	0.700	0.400	0.700	0.664	0.401
<b>PPEM</b>	64.955	18.000	31.938	52.115	65.806	65.338	75.000	15.769	29.519	26.890
<b>ERAT</b>	1.322	6.100	1.561	2.174	5.935	1.250	2.400	1.274	1.670	4.469
<b>FUEL</b>	19.909	30.037	20.979	21.890	29.007	19.898	25.786	20.125	21.644	28.539
<b>AIR</b>	178.961	804.397	185.255	291.781	717.919	169.866	241.505	175.085	233.944	500.000

**Table 4:** The bounds for different objectives calculated by stochastic old model multi-objective optimization

Extending on what was already mentioned in the introduction, the stochastic old model results are expected to be closer to the experimental values than the deterministic old model results. Now by replacing the old PEMFC and SOFC models with new ones, since the new models reduce the uncertainties and/or is more accurate, the deterministic new model MOP results should to a certain degree similar to the stochastic old model MOP results. The stochastic new model trade-off surface should also agree with the deterministic new model surface and to a greater degree. This would prove that the models are of sufficient complexity for the level of detail required for the overall flowsheet. An initial indication of the trend of similarity between the three cases: 1) stochastic old model MOP, 2) deterministic new model MOP and 3) stochastic new model MOP can be noticed in tables 4, 5 and 6 respectively. The new SOFC model stochastic optimization predicts current densities within a range of 210 – 735 mA/cm<sup>2</sup> as compared to a range of 70 – 850 mA/cm<sup>2</sup> predicted by the old model stochastic optimization and new model deterministic optimization. Though the new model stochastic optimization differs on the extreme ranges, it should be noted that within the range of 200 – 735 mA/cm<sup>2</sup>, the objectives for all designs for the three cases are within 20% of each other except on a few cases where they are otherwise. This anomaly can be attributed to the existence of multiple solutions.

	MAX	MIN	MIN	MIN	MAX	MIN	MAX	MIN	MIN	MAX
	ACEFF	ACEFF	CAP	COE	CO2EM	CO2EM	CDPEM	CDPEM	CDSOFC	CDSOFC
Design No.	1	2	3	4	5	6	7	8	9	10
<b>PWRTG</b>	1471.450	1482.950	1473.595	1471.958	1475.595	1469.537	1468.098	1458.403	1474.692	1468.575
<b>ACEFF</b>	0.723	0.473	0.649	0.652	0.497	0.710	0.561	0.712	0.711	0.502
<b>CAP</b>	2568.988	3503.311	2092.292	2107.947	6219.265	2752.843	1891.745	2420.518	2119.980	2910.327
<b>COE</b>	0.082	0.097	0.068	0.069	0.156	0.087	0.062	0.079	0.071	0.084
<b>CO2EM</b>	0.273	0.417	0.304	0.303	0.397	0.278	0.352	0.277	0.278	0.393
<b>CDSOFC</b>	75.301	814.996	202.020	210.970	854.701	69.013	693.001	85.005	105.697	866.026
<b>CDPEM</b>	45.841	37.580	42.841	45.235	51.808	46.300	53.566	33.323	39.962	46.169
<b>UTIL</b>	0.699	0.455	0.590	0.650	0.428	0.682	0.407	0.691	0.700	0.400
<b>PPEM</b>	63.329	19.129	37.180	53.000	65.718	63.573	75.000	18.165	34.944	38.491
<b>ERAT</b>	1.288	6.100	1.768	2.550	6.073	1.381	2.047	1.296	1.551	4.537
<b>FUEL</b>	20.118	30.984	22.446	22.331	29.359	20.460	25.873	20.250	20.504	28.945
<b>AIR</b>	176.849	838.736	228.225	361.109	744.192	188.154	210.527	176.983	217.202	512.635

**Table 5:** The bounds for different objectives calculated by deterministic new model multi-objective optimization

	MAX	MIN	MIN	MIN	MAX	MIN	MAX	MIN	MIN	MAX
	ACEFF	ACEFF	CAP	COE	CO2EM	CO2EM	CDPEM	CDPEM	CDSOFC	CDSOFC
Design No.	1	2	3	4	5	6	7	8	9	10
<b>PWRTG</b>	1499.525	1472.298	1416.973	1460.106	1448.738	1501.591	1469.467	1472.094	1467.093	1469.744
<b>ACEFF</b>	0.720	0.472	0.663	0.679	0.493	0.723	0.550	0.689	0.713	0.500
<b>CAP</b>	2653.190	3545.513	1766.678	2120.356	6342.055	2785.379	1886.987	2395.730	1702.580	2985.674
<b>COE</b>	0.080	0.098	0.061	0.069	0.159	0.083	0.063	0.074	0.060	0.086
<b>CO2EM</b>	0.274	0.418	0.298	0.291	0.400	0.273	0.359	0.286	0.277	0.394
<b>CDSOFC</b>	218.442	745.849	355.234	229.660	700.000	214.351	318.568	276.604	213.115	735.000
<b>CDPEM</b>	52.631	42.684	47.457	52.081	57.605	52.575	59.440	38.123	42.981	43.020
<b>UTIL</b>	0.693	0.450	0.606	0.694	0.430	0.696	0.400	0.650	0.700	0.479
<b>PPEM</b>	65.728	16.982	32.092	62.090	65.762	65.863	75.000	15.000	25.000	18.000
<b>ERAT</b>	1.261	7.000	1.560	2.330	6.093	1.261	2.400	1.296	1.459	5.131
<b>FUEL</b>	20.581	30.835	21.129	21.255	29.028	20.546	26.402	21.123	20.355	29.040
<b>AIR</b>	175.393	947.903	195.022	335.394	741.128	175.912	247.278	173.602	202.775	696.044

**Table 6:** The bounds for different objectives calculated by stochastic new model multi-objective optimization

These initial indications of similarity observed with the pay-off tables can be confirmed with the full Pareto surfaces. For reasons of comparison, the range of data corresponding to a CDS of 210 – 735 mA/cm<sup>2</sup> has been displayed. This comparison of Pareto surfaces would determine whether the higher level fuel cell models have enabled achieving a reasonable level of accuracy. Figure 9 compares the Pareto surfaces of the three objectives: ACEFF (x-axis), CO<sub>2</sub> emissions (y-axis) and CAP (z-axis) for the three cases: stochastic new model, deterministic new model and stochastic old model MOP. There is a general trend of green and yellowish green in all 3 surfaces and additionally there are also specific regions of similarity which have been highlighted. For example there is a 2400 \$/kW CAP region in the upper left corner of all surfaces corresponding to a CO<sub>2</sub>EM of around 0.38 kg/kWh and an overall efficiency of around 0.52. A 1800 \$/kW region can also be noted in the lower right corner of all surfaces, corresponding to a CO<sub>2</sub>EM of 0.28 kg/kWh and ACEFF of 0.70. There exists a 1400-1600 \$/kW region in the ACEFF range of 0.64-0.66 and CO<sub>2</sub>EM of around 0.30 kg/kWh. in all three surfaces. Finally we can see a 2200-2400 \$/kW area at an ACEFF of around 0.56 and CO<sub>2</sub>EM of 0.34 in the new deterministic and new stochastic surfaces, but is not present in the old stochastic surface. Figure 10 compares the Pareto surfaces of the three objectives: ACEFF (x-axis), CDSOFC (y-axis) and CAP (z-axis) for the three cases: stochastic new model, deterministic new model and stochastic old model MOP. The first impression when the surfaces are seen together is the overall similarity in the color trends - region of blue and dark green in the right hand area and region of light green and yellow in the left hand area of all three surfaces. There is a 2200-2400 \$/kW region corresponding to a CDS of 350-500 mA/cm<sup>2</sup> and ACEFF of 0.55-0.58 in the old model stochastic surface. The same region, but with a slightly decreased CAP can also be seen in the new model deterministic and stochastic surfaces, though they are split into 2 separate regions. Another region of similarity between the new model stochastic and deterministic is the 2200-2400 \$/kW region in upper left corner of the surface corresponding to high CDS and low efficiency. This trend is faintly noticeable in the old stochastic surface where this particular region is light green in color and on the verge of turning yellowish. There is also a 2000 \$/kW region around an efficiency range of 0.64-0.66 and CDS of 290 mA/cm<sup>2</sup> present in all three surfaces. The comparison of these 2 sets of Pareto surfaces provide sufficient evidence that the current higher level models for the SOFC and PEMFC are sufficiently complex for the SOFC-PEM flowsheet to obtain reasonable multi-objective optimal designs and trade-off surfaces.

In this paper, we have shown only 2 sets of Pareto surfaces but these trends are observed for the trade-off surfaces of all objectives and designs. The extent of closeness between the old stochastic, new deterministic and new stochastic, more so between the latter two leads to the conclusion that through utilization of the new SOFC and PEMFC models, an optimal limit of accuracy has been reached and using more complex models would not provide any significant enhancement of predicted results.

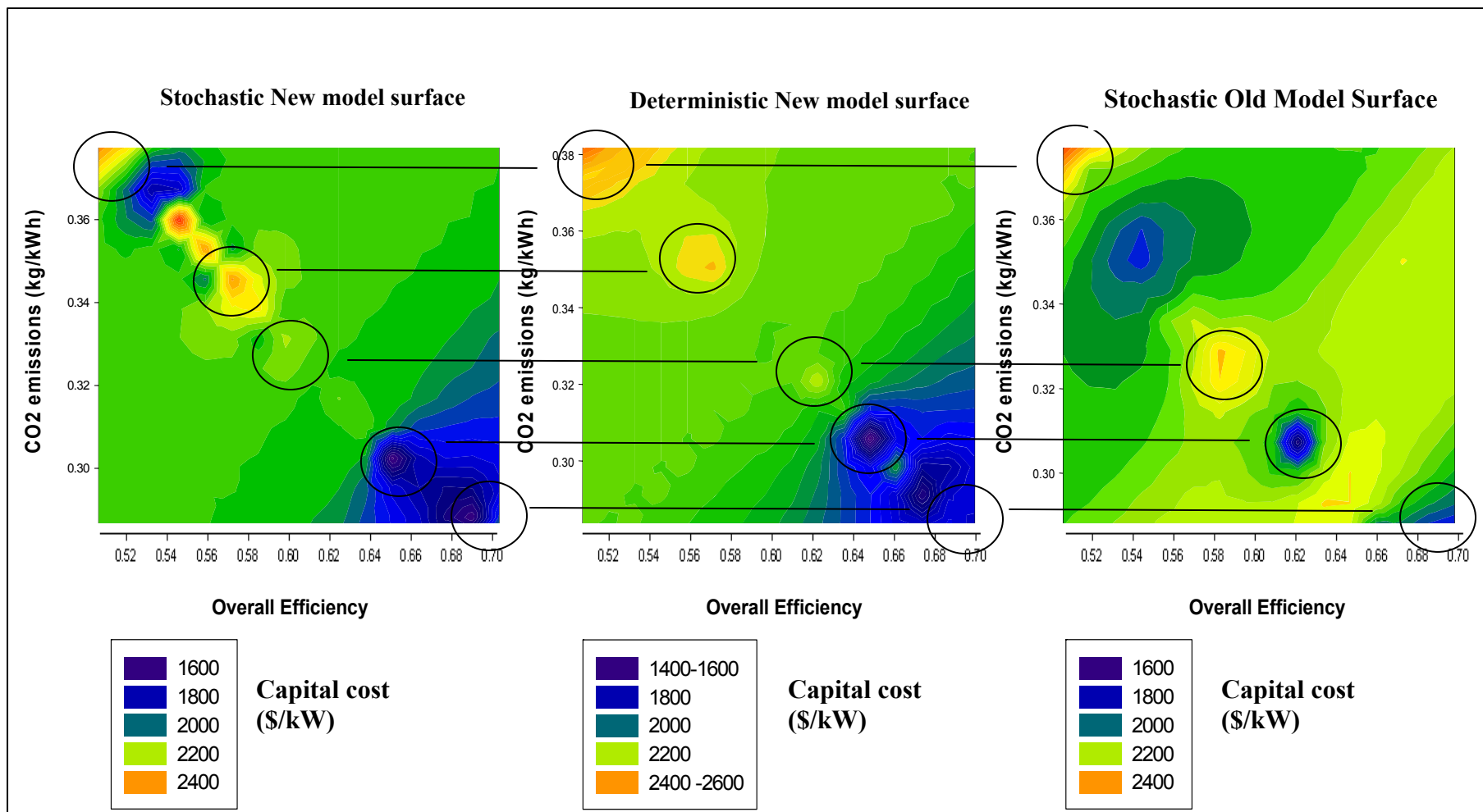


**Figure 9:** Comparison of the Pareto surfaces for the three objectives: ACEFF, CO2EM and CAP



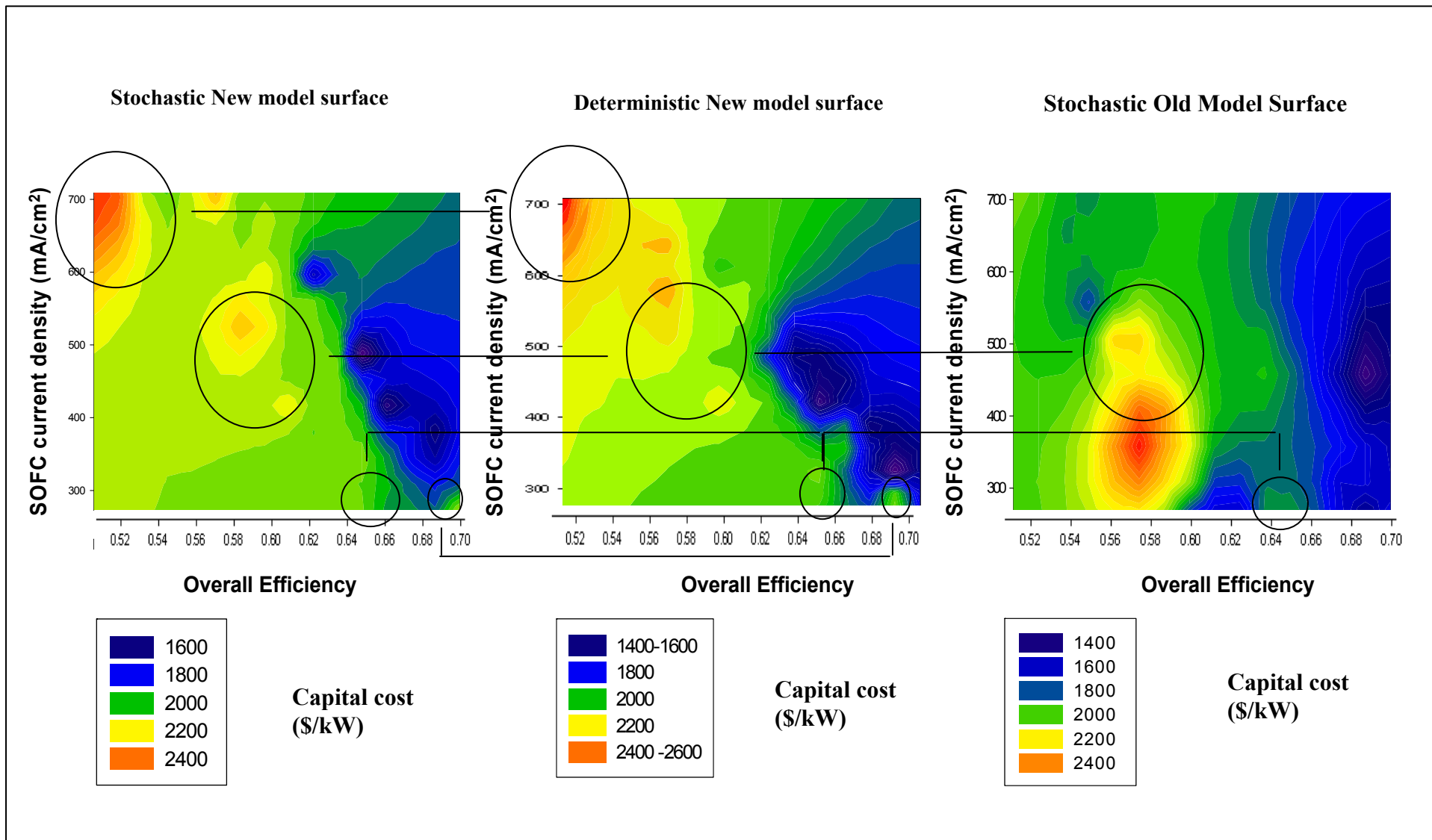


**Figure 10:** Comparison of the Pareto surfaces for the three objectives: ACEFF, CDS and CAP

## **5. Conclusions**

In this work, we are identifying the optimal model complexity given that system level models tend to have uncertainties. This is achieved by accurately characterizing, and quantifying uncertainties in different levels of models. The models are chosen based on the uncertainty reductions they offer. The optimal complexity is checked based on the comparison of deterministic and stochastic Pareto surfaces in a multi-objective setting. In this work, we have dealt with the system level models of SOFC and PEMFC for a hybrid power plant design. The solution of an MOP is not a single solution but a Pareto surface. To obtain these Pareto surfaces for deterministic and stochastic analysis, we needed an efficient framework. This framework is based on efficient algorithms like the MINSOOP algorithm for multi-objective optimization, and efficient sampling techniques for uncertainty analysis. The pay-off table, a first approximation to Pareto surface, results gave an initial indication of similarity between the designs. Finally we performed the full-fledged optimization, computed and plotted the trade-offs and compared the three surfaces: 1) old stochastic, 2) new deterministic and 3) new stochastic. Through this comparison we found a consistent trend of similarity between the surfaces of all three cases, more so between the new deterministic and new stochastic designs. The agreement between the three surfaces especially between the new stochastic and new deterministic proved that through the use of these new models, we have identified models with the optimal complexity for the system level flowsheet and employing more intricate models for the fuel cells would not result in any significant improvement of output predictions.

## **Acknowledgements**

The funding for this work is provided by National Energy Technology Laboratories, NETL/DOE, Morgantown, WV and thanks to Francesco Baratto for the new SOFC model.

## **References**

1. National Energy Technology Laboratory (NETL), 'Aspen Plus – Fluent Integration toolkit document', 2004.
2. Diwekar, U. M.; Introduction to Applied Optimization, *Kluwer Academic Publishers*, Dordrecht, 2003.
3. Subramanyan, K., Diwekar U. and Goyal A.; 'Multi-objective optimization of hybrid fuel cell power system under uncertainty', *Journal of Power Sources*, 132, 99-112, 2004.
4. AspenTech, Aspen Plus Documentation Version 11.1; AspenTech: Cambridge, MA, 2002.
5. AspenTech, Aspen Plus Documentation Version 12.1; AspenTech: Cambridge, MA, 2003.
6. Petruzzi L., Cocchi, S., and Fineschi, F.; 'A global thermo-electrochemical model for SOFC systems design and engineering', *Journal of Power Sources* 118, 96-107, 2003.

7. US Department of Energy; *Fuel cell handbook*, Fifth edition, 2000.
8. Geisbrecht R.; 'Theory based process modeling for evaluation of fuel cells in advanced energy systems', *AIChE Spring 2002 National Meeting*, New Orleans, LA, 2002.
9. Aguiar, P., Chadwick, D., and Kershenbaum, L.; 'Modelling of an indirect internal reforming solid oxide fuel cell', *Chemical Engineering Science*. 57(10),1665-1677, 2002.
10. Campanari, S.; 'Thermodynamic model and parametric analysis of a tubular SOFC module', *Journal of Power Sources*, 92, 26-34, 2001.
11. Chan, S. H., Khor, K.A., and Xia, Z.T.; 'A complete polarization model of a solid oxide fuel cell and its sensitivity to the change of cell component thickness', *Journal of Power Sources*, 93, 130-140, 2001.
12. Cownden R., Nahon, M., and Rosen M.A.; 'Modelling and analysis of a solid polymer fuel cell system for transportation applications', *International Journal of Hydrogen Energy*, 26, 615-623, 2001.
13. Nagata, S., Momma, A., Kato, T., and Kasuga, Y.; 'Numerical analysis of output characteristics of tubular SOFC with internal reformer', *Journal of Power Sources*, 101(1), 60-71, 2001.
14. Xui-Mei, G, Hidajat, K., and Ching, C.; 'Simulation of a solid oxide fuel cell for oxidative coupling of methane', *Catalysis Today*, 50, 109-116, 1999.
15. Virkar A.V., Chen, J., Tanel, C.W., and Kim, J.; 'The role of electrode microstructure on activation and concentration polarizations in solid oxide fuel cells' *Solid State Ionics*, 131,189-198, 2000.
16. Al-Qattan A. M., Chmielewski, D.J., Al-Hallj, S. and Selman, J.R.; 'A novel design for solid oxide fuel cell stacks' *Chemical Engineering Science*, 59, 131-137, 2004.
17. Hall, D. J. and Colclaser, R.G.; 'Transient Modeling and Simulation of a Tubular Solid Oxide Fuel Cell, *IEEE Transactions on Energy Conversion*, 14, 749-753, 1999..
18. Maggio, G., Recupero, V., and Pino, L.; 'Modeling polymer electrolyte fuel cell: an innovative approach', *Journal of Power Sources*, 101, 275-286, 2001.
19. Arthur D. Little, Inc.: Conceptual Design of POX/SOFC 5kW net System. Final report to Department of Energy National Energy Technology Laboratory. 2001.
20. Diwekar, U.M., Rubin, E.S., and Frey, H.C.; "Optimal Design of Advanced Power Systems Under Uncertainty," *Energy Conversion and Management Journal*, 38, 1725-1735, 1997.
21. Subramanyan, K., and Diwekar U.; 'Characterization and quantification of uncertainty in solid oxide fuel cell hybrid power plants', *Journal of Power Sources*, 142, 103-116, 2005.
22. Kalagnanam, J. R. and Diwekar, U.M.; 'An Efficient Sampling Technique for Off-line Quality Control', *Technometrics*, 3, 308-319, 1997.
23. Fu, Y and Diwekar, U.M.; 'An Efficient Sampling Approach to Multi-objective Optimization', *Annals of Operations Research (in press)*. 2004.